



Theoretical Studies on Reactivity Indices, Electronic, Optical and Thermodynamic Properties of Pentacene-Tetrapyrrole Derivatives using DFT Method

MANISHA¹, VIJAY DANGI^{1,*} and BRAHAMDUTT ARYA^{2,3,*}

¹Department of Chemistry, Baba Mastnath University, Asthal Bohar, Rohtak-124021, India

²Y & Y Nanotech Solutions Pvt. Ltd., Rohtak-124001, India

³Department of Higher Education, Sector-5, Shiksha Sadan, Panchkula-134114, India

*Corresponding authors: E-mail: vijaydangi@bmu.ac.in; brahmdattarya@gmail.com

Received: 8 April 2024;

Accepted: 18 June 2024;

Published online: 30 August 2024;

AJC-21722

A detailed theoretical analysis of the electronic properties, reactivity indices, optical and thermodynamic properties of pentacene-tetrapyrrole (PTP) molecules utilizing the DFT and TD-DFT methods at 6-311(d,p) basis set is conducted. The thermodynamic properties and molecule electrostatic potential were computed using the DFT/B3LYP/6-311(d,p) technique. The electronic properties, reactivity indices and optical properties were determined using the TD-DFT/6-311(d,p) at several functionals: B3LYP, CAM-B3LYP, B3PW91, PBEPBE and WB97XD. The change in electronic properties, reactivity indices, optical and thermodynamic properties were also investigated with variation in the position of the -NH group at the pentacene's periphery from inward to outward and central benzene ring of pentacene with nitrogen containing cyclic rings such as pyrrole in pentacene-tetrapyrrole derivatives.

Keywords: Pentacene-Tetrapyrrole molecules, DFT, TD-DFT, Optoelectronic, Thermodynamic, Pentacene.

INTRODUCTION

The efficiency and effectiveness of organic electronic devices, as well as their prospective uses, have recently been shown to have the potential to increase energy consumption and output. These electronic devices include electronic, optoelectronic and photovoltaic applications [1-4], which have been commonly used in sensors [5-7], photodetectors [8], transistors [9], organic light-emitting diodes [10,11] and large-area integrated circuits [12]. Organic compounds based on polycyclic aromatic hydrocarbons are currently gaining popularity due to their potential applications in nanotechnology and optoelectronics [13-17]. However, the optoelectronic properties of polycyclic aromatic hydrocarbons are significantly influenced by their size, shape and periphery substitution [18-22]. The insertion of heteroatoms like nitrogen into the polycyclic aromatic framework is another effective method for improving their essential chemical as well as physical characteristics, such as lowering the lowest unoccupied molecular orbitals, *etc.* [23-26].

Bunz [27] investigated the electric properties and application in electronic devices of larger linear *N*-heteroacenes,

referred to as azaacenes. The results revealed that the insertion of nitrogen atoms to the aromatic moiety of acenes stabilizes their frontier molecular orbitals and raises their electron affinity. Moreover, by increasing the number of nitrogen atoms, attaching electronegative substituents and extending the π -perimeter on azaacenes, increasing their electron affinity while reduction potential decreases [27]. Moreover azaacenes, such as *bis*(triisopropylsilylethynyl)-substituted tetraazapentacene with symmetrical properties, are extensively employed in organic field effect transistors. However, smaller azaacenes are also effective as organic light-emitting diodes (OLEDs).

Diazatetracenes and modified benzoquinoxalines compared to pure tetracene are successful in improving electron injection and OLED brightness. Furthermore, the addition of oligocene units *e.g.* benzene, naphthalene, anthracene, tetracene, pentacene and heptacene) attached at the end cores of 2,5-di(pyrimidine-5-yl)thieno[3,2-*b*]thiophene results in the enhancement of the optoelectronic properties as reported by Irfan *et al.* [28]. The oligocene units are able to inject charges because their electron affinity is high, while their ionization potential and energy gap are low.

The optical property suggest that these compounds might be good near-infrared and visible emitters. Vidya & Chetti [29] investigated the effects of polycyclic aromatic hydrocarbons and heteroatomic bridges (N, S and O) on the optoelectronic characteristics of 1,3,5-triazine based derivatives. Addition of aromatic rings along the molecular axis in the Y-direction results in an increase in the energy gap and a shift in the absorption maxima towards the shorter wavelength while adding the aromatic rings one after the other without a bridge along the molecular axis in the X-direction decreases the energy gap and shifts the absorption maxima towards the longer wavelength. In another study, Tri *et al.* [30] examined the optoelectronic properties of unsubstituted heptacene, its fluorinated derivatives and thiophene, silol analogues. They found that unsubstituted heptacene can be employed as a p-type semiconductor, whereas fluorinated derivatives can be used as n-type semiconductors. The electronic absorption shifting occurred towards red light for fluorinated derivatives, blue light for thiophene derivatives and red light for silol derivatives as compared to unsubstituted heptacene.

The improvement of the optoelectronic properties of organic materials, insertion of heteroatoms and periphery substitution into the organic materials framework would be an excellent agreement. In this work, we have designed six derivatives of pentacene-tetrapyrrole (PTP) and investigated the effect of the exchange position of the -NH group at the pentacene's periphery from inward to the outward and central benzene ring of pentacene with nitrogen containing cyclic rings in pentacene-tetrapyrrole molecules on the electronic properties, reactivity indices, optical and thermodynamic properties. The DFT and

TD-DFT approaches were used to calculate all of these properties at 6-311(d,p) in the gaseous state. TD-DFT/6-311(d,p) was used to evaluate electronic properties, reactivity indices and optical properties at plenty of functionals: B3LYP, CAM-B3LYP, B3PW91, PBEPBE and WB97XD.

EXPERIMENTAL

Designed molecular structures: As in Fig. 1, four pyrrole rings were affixed at the periphery of pentacene in PTP1 and PTP2. The only difference between molecules PTP1 and PTP2 is that the -NH group presents inward and outward, respectively. Furthermore, replace the central benzene ring of pentacene with nitrogen containing cyclic rings in pentacene-tetrapyrrole molecules (in PTP1 and PTP2). PTP3 and PTP5 molecules develop with the help of PTP1 molecule, whilst PTP4 and PTP6 molecules are made with the help of PTP2 molecule by substituting the core benzene ring of pentacene with nitrogen containing cyclic rings in the PTP molecules. As a result, PTP1, PTP3 and PTP5 compounds have -NH groups facing inside while PTP2, PTP4 and PTP6 compounds have -NH groups facing outside. Furthermore, the effect of the swap of the NH group's position at the pentacene's periphery from inward to outward as well as the central benzene ring of pentacene with nitrogen containing cyclic rings in PTP molecules, on electronic properties, reactivity indices, optical and thermodynamic properties was investigated.

Computational methods: All calculations in this study were carried out using the Gaussian software package [31]. The structures of the designed PTP derivatives were optimized using the molecular mechanics, semi-empirical approach at PM6 level

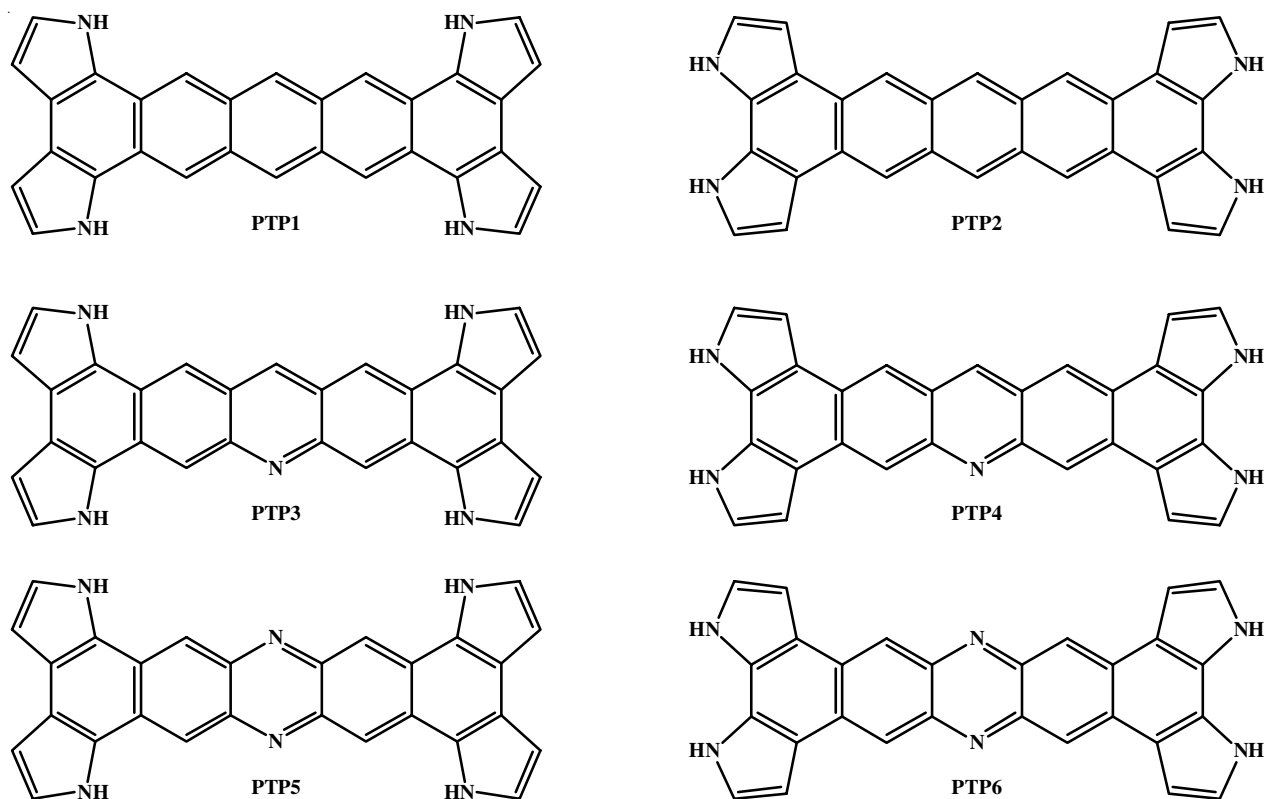


Fig. 1. Structure of designed pentacene-tetrapyrrole (PTP) molecules

and DFT method at B3LYP/6-311(d,p) levels of theory in gaseous state. Semiempirical and DFT approaches were used to optimize the structure of the PTP derivatives with frequency, resulting in the identification of structures at minima on the potential energy surface. The thermodynamic characteristics and electrostatic potential mapping of PTP derivatives were determined using the DFT-optimized structures approach at the B3LYP/6-311(d,p) theoretical levels. The TD-DFT approach was employed on ground state optimized structures to examine the frontiers molecular orbitals and optical properties at a variety of functionals: B3LYP, CAM-B3LYP, B3PW91, PBEPBE and WB97XD with 6-311 (d,p) basis set. Furthermore, using the frontiers molecular orbital energies, the energy gap between frontiers molecular orbitals and chemical reactivity indices was calculated. The Gauss Sum software [32] was used to determine the total density of state results for PTP molecules.

Reactivity indices: The energy band gap is the difference between the lowest unoccupied molecular orbitals (LUMO) and the highest occupied molecular orbitals (HOMO), which can be calculated using the following formula:

$$E_g = E_{\text{LUMO}} - E_{\text{HOMO}} = \text{IP} - \text{EA} \quad (1)$$

The following formulas were employed to determine the reactivity indices, which include ionization potential, electron affinity, electronegativity, hardness, softness, chemical index, electrophilicity index, electrodonating power, electroaccepting power, net electrophilicity and nucleophilicity index:

The energies of the HOMO and LUMO orbitals were used to calculate the ionization potential and electron affinity:

$$\text{IP} = -E_{\text{HOMO}} \quad (2)$$

$$\text{EA} = -E_{\text{LUMO}} \quad (3)$$

The chemical hardness was obtained by half of the energy band gap [33], whereas the chemical softness is inversely related to chemical hardness [34]:

$$\eta = \frac{(\text{IP} - \text{EA})}{2} \quad (4)$$

$$\xi = \frac{2}{(\text{IP} - \text{EA})} = \frac{1}{\eta} \quad (5)$$

The electronegativity [33] and the chemical potential were obtained using eqns. 6 and 7, respectively:

$$\chi = \frac{(\text{IP} - \text{EA})}{2} \quad (6)$$

$$\mu = -\left(\frac{\text{IP} + \text{EA}}{2}\right) = -\chi \quad (7)$$

The electrophilicity index was obtained using the following formula [34,35]:

$$\omega = \frac{\mu^2}{2\eta} \quad (8)$$

The electrodonating power, electroaccepting power and net electrophilicity were obtained using eqn. 9-11, respectively [36,37]:

$$\omega^- = \frac{(3\text{IP} + \text{EA})^2}{16(\text{IP} - \text{EA})} \quad (9)$$

$$\omega^+ = \frac{(\text{IP} + 3\text{EA})^2}{16(\text{IP} - \text{EA})} \quad (10)$$

$$\omega^{+/-} = \omega^+ - (-\omega^-) = \omega^+ + \omega^- \quad (11)$$

The nucleophilicity index (NI) [38-41] was calculated using the following formula:

$$\text{NI} = -\text{IP} \quad (12)$$

RESULTS AND DISCUSSION

Optimized structures: The structures of pentacene-tetrapyrrole (PTP) molecules were initially optimized using molecular mechanics, afterward reoptimized using the semi-empirical approach at the PM6 functional and at last optimized using density functional theory (DFT) using the 6-311(d,p) basis set/B3LYP functional. These DFT-optimized structures contain zero imaginary frequency, indicating that they have been fully optimized and identified on minimum-energy surfaces. Fig. 2 and Table-1 present the DFT-optimized structures and ground state energies of PTP molecules, respectively. Replacement of the -NH group from inward (PTP1, PTP3 and PTP5) to outward (PTP2, PTP4

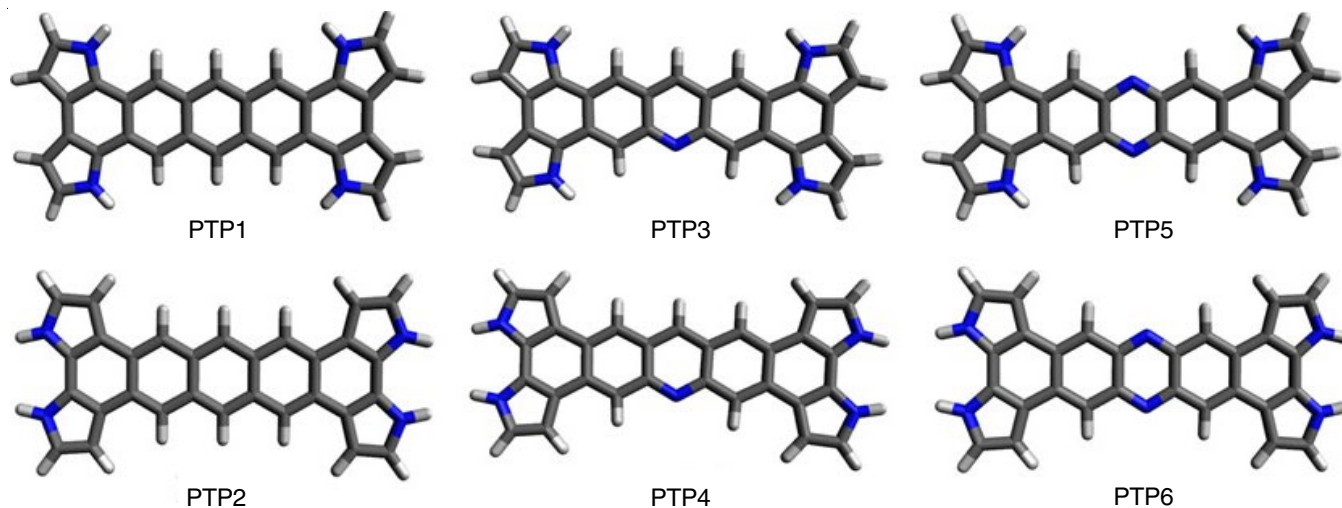


Fig. 2. DFT optimized structures of pentacene-tetrapyrrole (PTP) molecules using B3LYP/6-311(d,p) level

TABLE-1
GROUND STATE TOTAL ENERGIES OF PTP
MOLECULES USING DFT/B3LYP/6-311(d,p) level

Compounds	Ground state total energy (a.u)
PTP1	-1373.40548778
PTP2	-1373.39745537
PTP3	-1389.45159329
PTP4	-1389.44266066
PTP5	-1405.49397478
PTP6	-1405.48406968

and PTP6) increases the ground state energy. The ground state energy decreases if the core benzene ring of pentacene in PTP1 and PTP2 is replaced by nitrogen containing cyclic rings (PTP3, PTP4, PTP5 and PTP6). The ground state energy order is as follows: PTP2 > PTP1 > PTP4 > PTP3 > PTP6 > PTP5. The predicted outcomes demonstrate that PTP5 molecule is the most stable because it exhibits the lowest ground-state energy among all the PTP molecules.

Electronic properties: The frontier molecular orbitals, known as lowest unoccupied molecular orbitals (LUMO) and highest occupied molecular orbitals (HOMO), play a crucial role in optical and electrical properties [42]. In general, when a molecule has a small energy gap between the HOMO and LUMO, then it has more charge transfer tendency. The higher the energy of HOMO, the easier it is to donate electrons and lower the energy of LUMO, the easier it is to accept electrons. The energies of frontier molecular orbitals and their electronic density distribution patterns were computed using the TD-DFT/6-311(d,p) level of theory at B3LYP, CAM-B3LYP, B3PW91, PBEPBE and WB97XD functionals in the gaseous phase and the energy gap. In the B3LYP functional, the HOMO and LUMO energies of PTP molecules are in order: PTP2 > PTP4 > PTP1

> PTP6 > PTP3 > PTP5. The order of HOMO and LUMO energies in CAM-B3LYP, B3PW91, PBEPBE and WB97XD functionals is the same as in B3LYP functional. The trend of the HOMO-LUMO energy gap in B3LYP and CAM-B3LYP is PTP2 > PTP4 > PTP6 > PTP1 > PTP3 > PTP5 and PTP4 > PTP2 > PTP1 > PTP6 > PTP3 > PTP5 whereas, order of the HOMO-LUMO energy gap in PBEPBE is: PTP2 > PTP4 > PTP1 > PTP6 > PTP3 > PTP5. The order of the HOMO-LUMO energy gap in B3PW91 and WB97XD functionals is the same as in the B3LYP functional. The NH group is switched from inward (PTP1, PTP3 and PTP5) to outward (PTP2, PTP4 and PTP6), which increases the HOMO-LUMO energy gap as well as HOMO and LUMO (destabilized the HOMO and LUMO) energy levels. PTP3/PTP4 and PTP5/PTP6 compounds show lower HOMO, LUMO levels and reduced HOMO-LUMO energy gap when the core benzene ring of pentacene in PTP1 and PTP2 is replaced by the nitrogen containing cyclic rings, pyridine and pyrazine, respectively. Because of its strong electron-withdrawing tendency and inductive effect, the nitrogen atom's insertion into the core benzene ring of pentacene in PTP1 and PTP2 (benzene → pyridine) stabilized the frontier molecular orbitals. The strong electronegativity of the nitrogen atom creates an inductive effect that stabilizes the frontier molecular orbitals when the number of nitrogen atoms increases (from benzene → pyridine → pyrazine or benzene → pyrazine). The LUMO energy of PTP molecules is greater than TiO₂ (4.01 eV) conduction band [43] (Fig. 3), allowing electrons to freely pass through the semiconductor substrate. Table-2 reveal that PTP5 molecule has the highest charge transfer tendency among all PTP molecules due to its lowered HOMO-LUMO energy gap. Further, the core region of the compounds under study contains most of the electronic density in the HOMO and LUMO (Fig. 4).

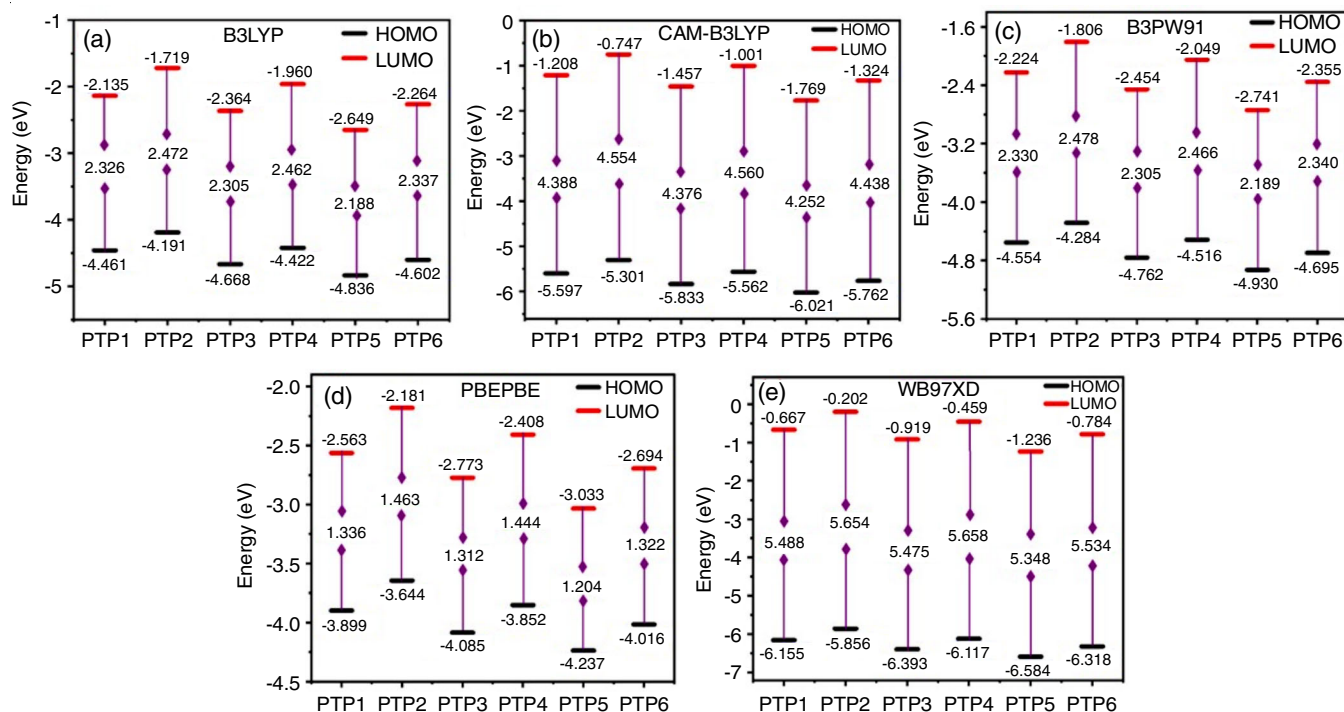


Fig. 3. Energies of HOMO, LUMO and HOMO-LUMO gap of pentacene-tetrapyrrole (PTP) molecules at several functionals B3LYP, CAM-B3LYP, B3PW91, PBEPBE and WB97XD using TD-DFT/6-311(d,p) level

TABLE-2
ENERGIES OF HOMO, LUMO AND HOMO-LUMO GAP OF DESIGNED PTP MOLECULES AT SEVERAL FUNCTIONALS B3LYP, CAM-B3LYP, B3PW91, PBEPBE AND WB97XD USING DFT/6-311(d,p) LEVEL

Functionals	E_{HOMO}	E_{LUMO}	E_g	E_{HOMO}	E_{LUMO}	E_g	E_{HOMO}	E_{LUMO}	E_g
	PTP1			PTP2			PTP3		
B3LYP	-4.461	-2.135	2.326	-4.191	-1.719	2.472	-4.668	-2.364	2.305
CAM-B3LYP	-5.597	-1.208	4.388	-5.301	-0.747	4.554	-5.833	-1.457	4.376
B3PW91	-4.554	-2.224	2.330	-4.284	-1.806	2.478	-4.762	-2.454	2.308
PBEPBE	-3.899	-2.563	1.336	-3.644	-2.181	1.463	-4.085	-2.773	1.312
WB97XD	-6.155	-0.667	5.488	-5.856	-0.202	5.654	-6.393	-0.919	5.475
	PTP4			PTP5			PTP6		
B3LYP	-4.422	-1.960	2.462	-4.836	-2.649	2.188	-4.602	-2.264	2.337
CAM-B3LYP	-5.562	-1.001	4.560	-6.021	-1.769	4.252	-5.762	-1.324	4.438
B3PW91	-4.516	-2.049	2.466	-4.930	-2.741	2.189	-4.695	-2.355	2.340
PBEPBE	-3.852	-2.408	1.444	-4.237	-3.033	1.204	-4.016	-2.694	1.322
WB97XD	-6.117	-0.459	5.658	-6.584	-1.236	5.348	-6.318	-0.784	5.534

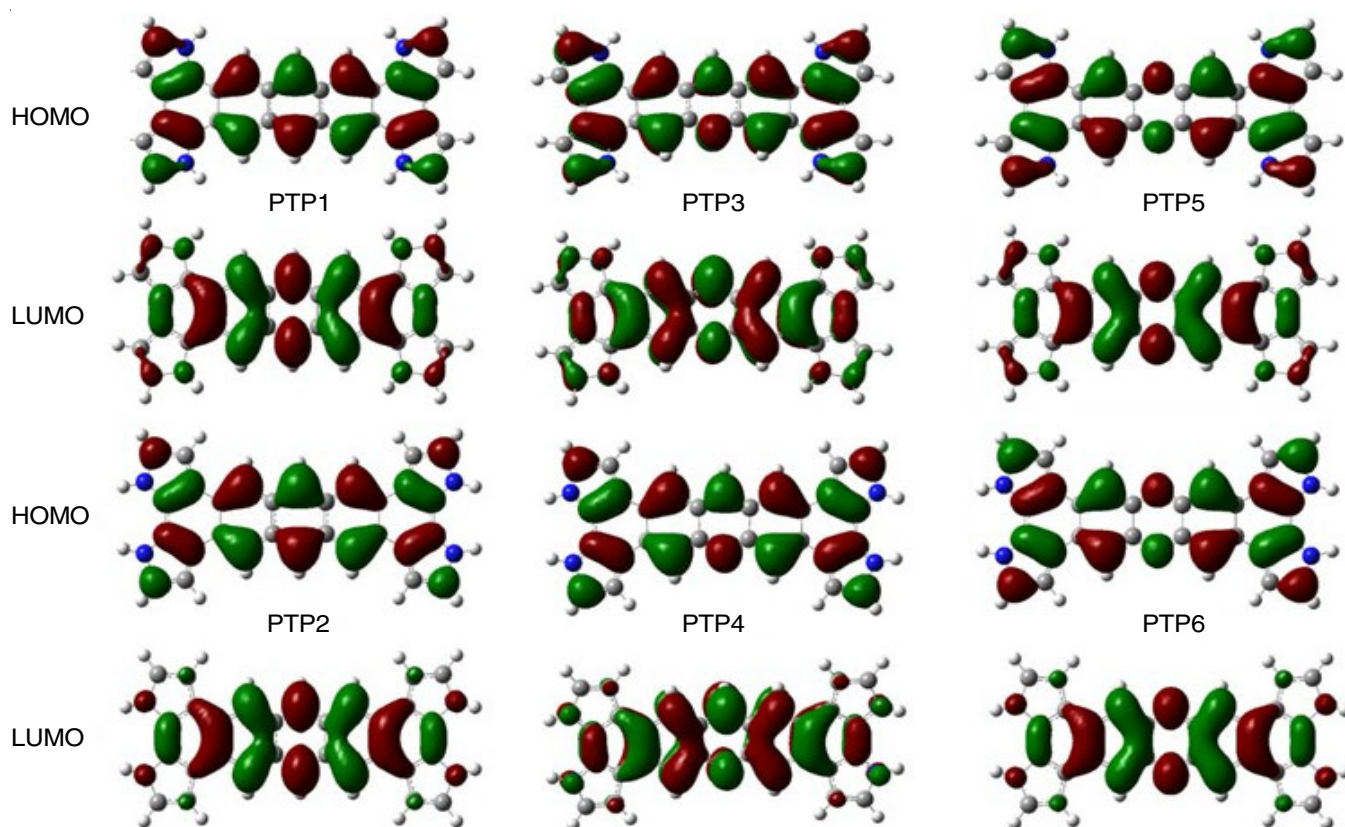


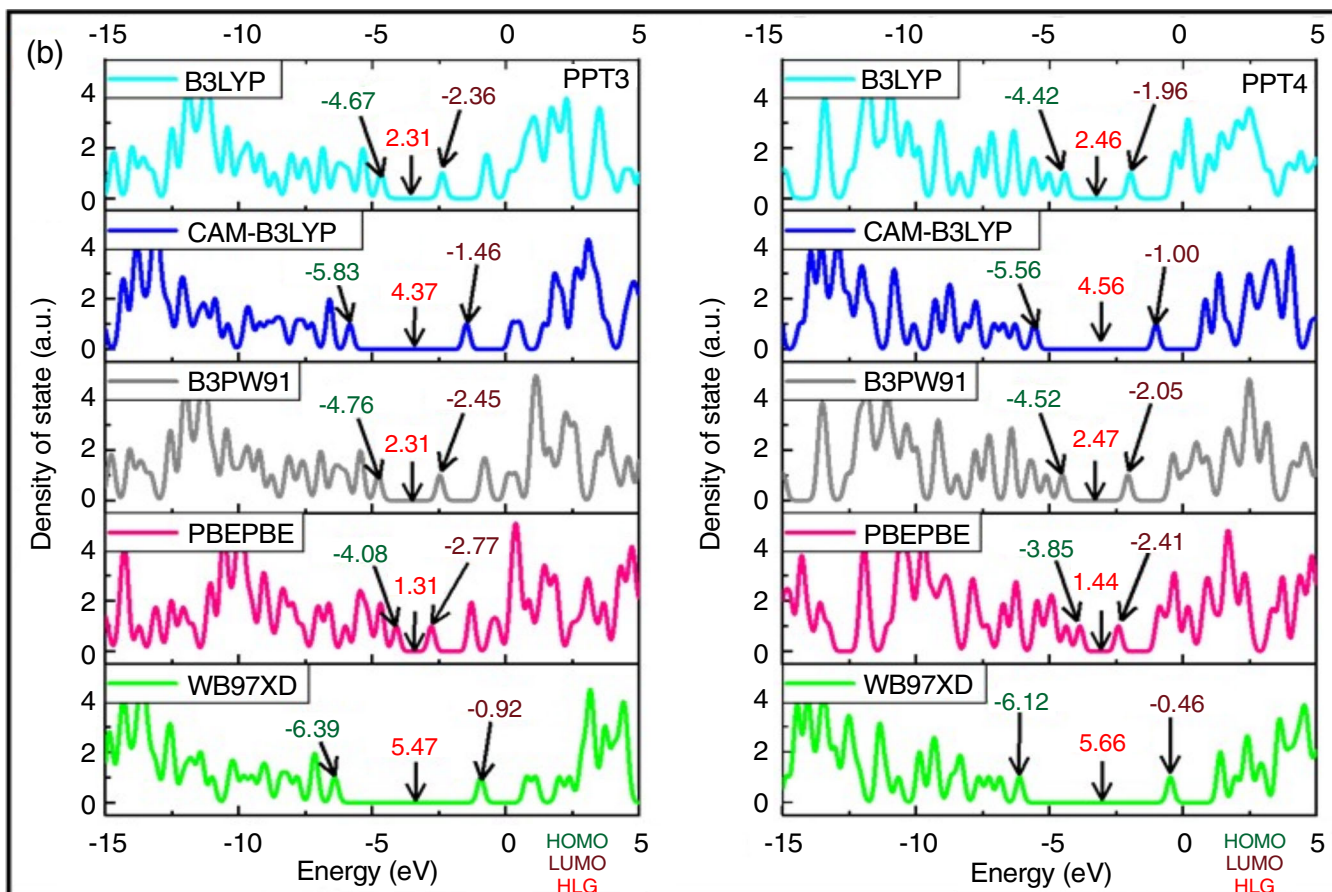
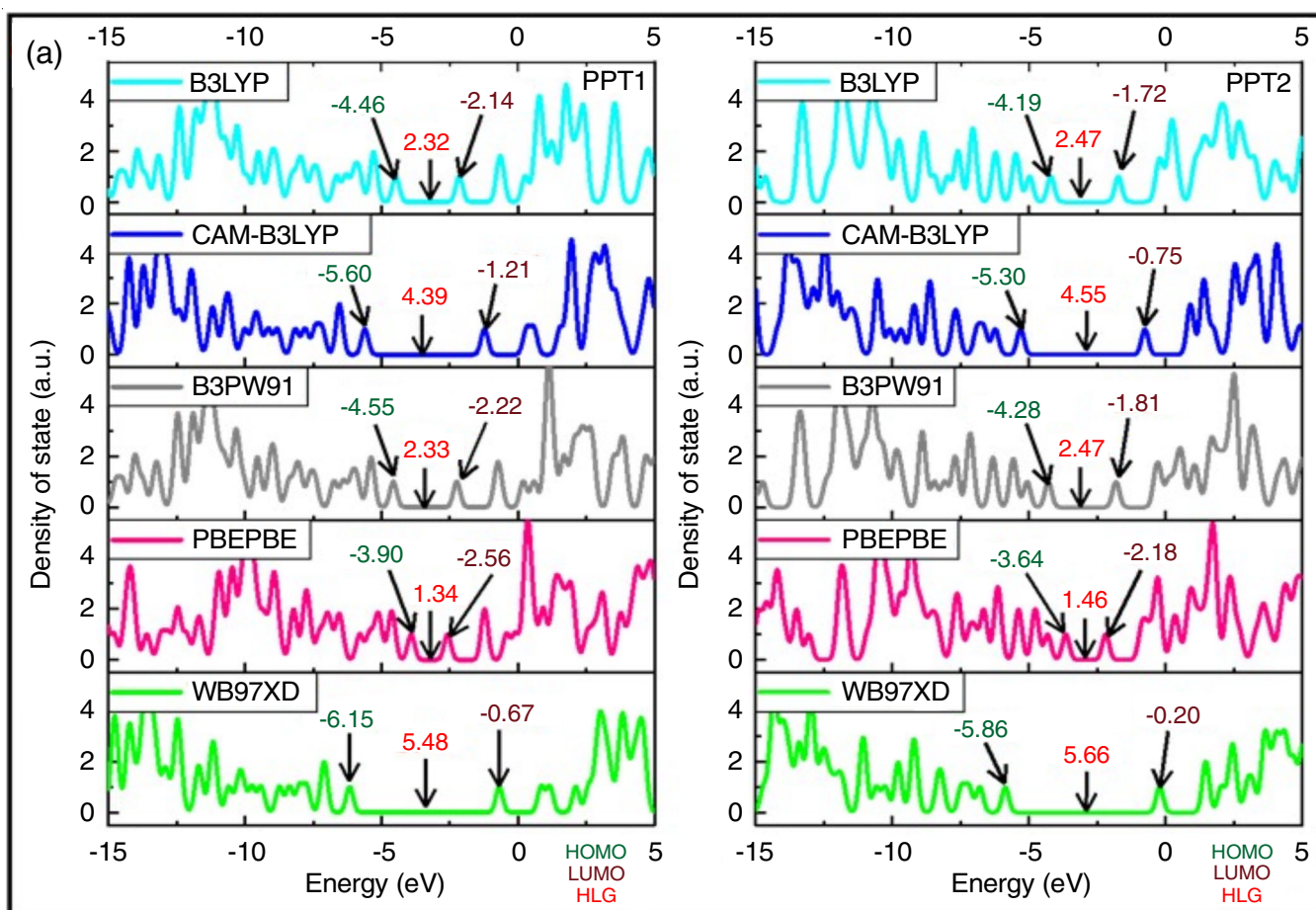
Fig. 4. Electron density distribution patterns of FMOs of PTP molecules using TD-DFTB3LYP/6-311(d,p) level

Density of states: The density of states for all designed compounds in several functionals *viz.* B3LYP, CAM-B3LYP, B3PW91, PBEPBE and WB97XD was estimated by employing the Gauss Sum software [32]. The density of state graph for all the PTP molecules is shown in Fig. 5. Consideration of both occupied and empty molecular orbitals is taken into consideration in this density of state analysis, which explains the validation of FMO results and accounts for any electronic transition. The density of states analysis for all the PTP molecules is quite consistent with the FMO results.

Reactivity indices: Reactivity indices, which include ionization potential, electron affinity, electronegativity, hardness, softness, chemical potential, electrophilicity index, electro-

donating power, electroaccepting power, net electrophilicity and nucleophilicity index, are useful for analyzing the reactivity and stability of molecule. The results of reactivity indices for PTP molecules are listed in Tables 3 and 4, respectively.

Ionization potential and electron affinity: The ability to lose and gain electrons is investigated using the ionization potential and electron affinity. Removing an electron becomes more challenging as the ionization potential increases, while adding an electron becomes more difficult as the electron affinity decreases. The ionization potential and electron affinity at B3LYP, CAM-B3LYP, B3PW91, PBEPBE and WB97XD functionals in the gaseous phase were calculated using the energies of frontier molecular orbitals. In the B3LYP functional, the ion-



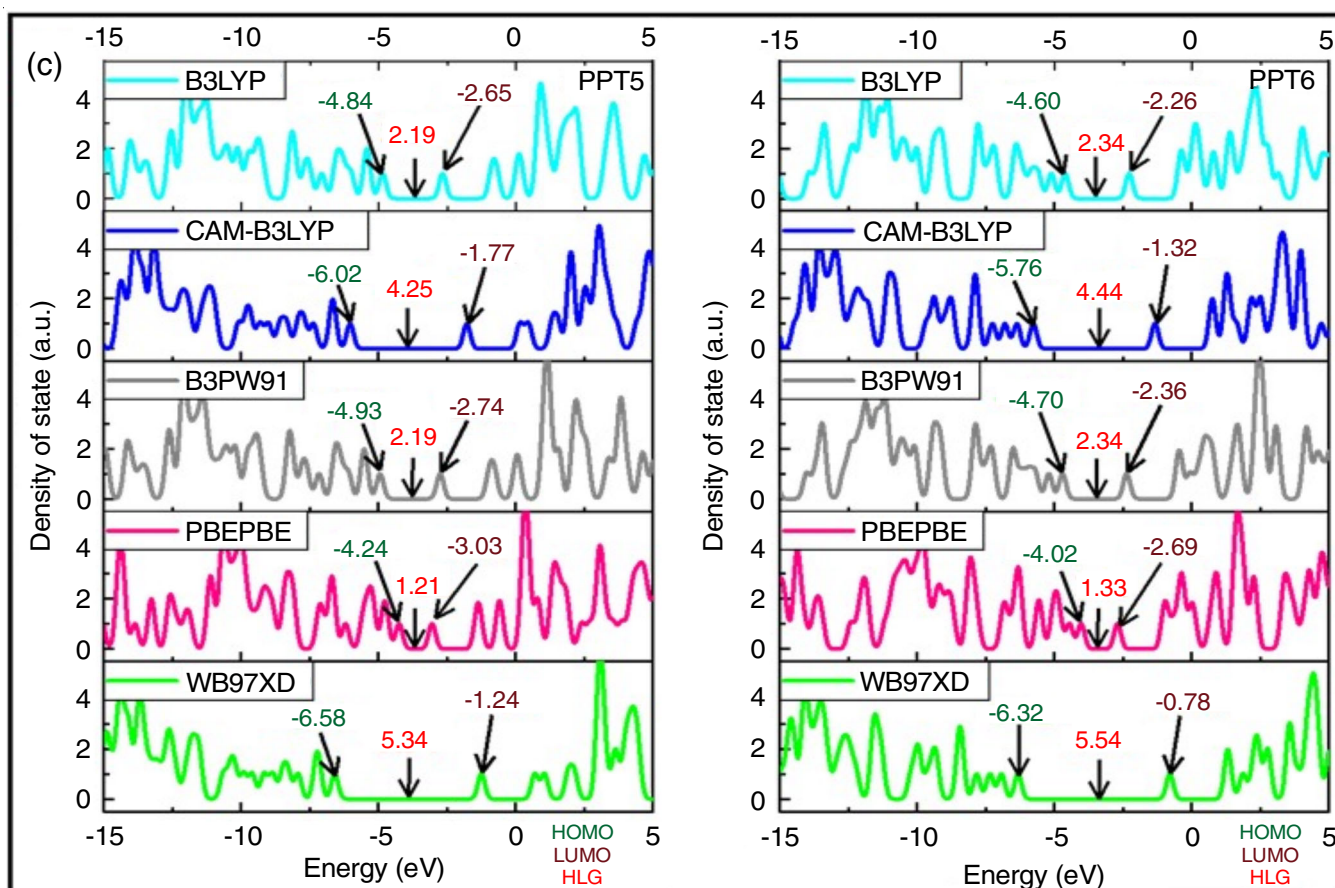


Fig. 5. Density of state of PTP molecules at several functionals B3LYP, CAM-B3LYP, B3PW91, PBEPBE and WB97XD using Gauss Sum software

TABLE-3
REACTIVITY INDICES SUCH AS IONIZATION POTENTIAL, ELECTRON AFFINITY, ELECTRONEGATIVITY, CHEMICAL POTENTIAL, HARDNESS AND SOFTNESS OF DESIGNED PTP MOLECULES AT SEVERAL FUNCTIONALS B3LYP, CAM-B3LYP, B3PW91, PBEPBE AND WB97XD USING TD-DFT/6-311(d,p) LEVEL

Functionals	IP	EA	χ	μ	η	ξ	IP	EA	χ	μ	η	ξ
PTP1							PTP2					
B3LYP	4.461	2.135	3.298	-3.298	1.163	0.430	4.191	1.719	2.955	-2.955	1.236	0.405
CAM-B3LYP	5.597	1.208	3.402	-3.402	2.194	0.228	5.301	0.747	3.024	-3.024	2.277	0.220
B3PW91	4.554	2.224	3.389	-3.389	1.165	0.429	4.284	1.806	3.045	-3.045	1.239	0.404
PBEPBE	3.899	2.563	3.231	-3.231	0.668	0.749	3.644	2.181	2.913	-2.913	0.731	0.684
WB97XD	6.155	0.667	3.411	-3.411	2.744	0.182	5.856	0.202	3.029	-3.029	2.827	0.177
PTP3							PTP4					
B3LYP	4.668	2.364	3.516	-3.516	1.152	0.434	4.422	1.960	3.191	-3.191	1.231	0.406
CAM-B3LYP	5.833	1.457	3.645	-3.645	2.188	0.229	5.562	1.001	3.281	-3.281	2.280	0.219
B3PW91	4.762	2.454	3.608	-3.608	1.154	0.433	4.516	2.049	3.282	-3.282	1.233	0.406
PBEPBE	4.085	2.773	3.429	-3.429	0.656	0.762	3.852	2.408	3.130	-3.13	0.722	0.693
WB97XD	6.393	0.919	3.656	-3.656	2.737	0.183	6.117	0.459	3.288	-3.288	2.829	0.177
PTP5							PTP6					
B3LYP	4.836	2.649	3.742	-3.742	1.094	0.457	4.602	2.264	3.433	-3.433	1.169	0.428
CAM-B3LYP	6.021	1.769	3.895	-3.895	2.126	0.235	5.762	1.324	3.543	-3.543	2.219	0.225
B3PW91	4.930	2.741	3.835	-3.835	1.095	0.457	4.695	2.355	3.525	-3.525	1.170	0.427
PBEPBE	4.237	3.033	3.635	-3.635	0.602	0.831	4.016	2.694	3.355	-3.355	0.661	0.756
WB97XD	6.584	1.236	3.910	-3.910	2.674	0.187	6.318	0.784	3.551	-3.551	2.767	0.181

ization potential and electron affinity of PTP derivatives are in order: PTP2 < PTP4 < PTP1 < PTP6 < PTP3 < PTP5. The order of the ionization potential and electron affinity in CAM-B3LYP, B3PW91, PBEPBE and WB97XD functionals is the same as in B3LYP functional. The -NH group is switched from

inward (PTP1, PTP3 and PTP5) to outward (PTP2, PTP4 and PTP6), which decreases the ionization potential and electron affinity (Fig. 6). It suggests that more difficult to add an electron and easier to remove an electron if the position of -NH group is altered at the periphery of pentacene. The ionization potential

TABLE-4
 REACTIVITY INDICES SUCH AS ELECTROPHILICITY INDEX, ELECTRO-DONATING POWER, ELECTRO-ACCEPTING POWER, NET ELECTROPHILICITY AND NUCLEOPHILICITY INDEX OF DESIGNED PTP MOLECULES AT SEVERAL FUNCTIONALS B3LYP, CAM-B3LYP, B3PW91, PBEPBE AND WB97XD USING TD-DFT/6-311(d,p) LEVEL

Functionals	ω	ω^+	ω^-	$\omega^{+/-}$	Nu	ω	ω^+	ω^-	$\omega^{+/-}$	Nu
		PTP1					PTP2			
B3LYP	4.677	6.345	12.941	19.286	-4.461	3.532	4.419	10.329	14.747	-4.191
CAM-B3LYP	2.638	2.422	9.229	11.651	-5.597	2.008	1.561	7.609	9.171	-5.301
B3PW91	4.929	6.761	13.539	20.3	-4.554	3.742	4.748	10.838	15.586	-4.284
PBEPBE	7.814	12.564	19.026	31.59	-3.899	5.804	8.873	14.702	23.574	-3.644
WB97XD	2.120	1.515	8.337	9.852	-6.155	1.623	0.923	6.981	7.904	-5.856
	PTP3					PTP4				
B3LYP	5.364	7.503	14.535	22.038	-4.668	4.136	5.388	11.77	17.159	-4.422
CAM-B3LYP	3.036	2.974	10.264	13.238	-5.833	2.361	2.011	8.575	10.586	-5.562
B3PW91	5.640	7.961	15.177	23.138	-4.762	4.368	5.763	12.331	18.094	-4.516
PBEPBE	8.962	14.659	21.517	36.176	-4.085	6.785	10.62	16.88	27.499	-3.852
WB97XD	2.442	1.912	9.224	11.136	-6.393	1.911	1.241	7.817	9.057	-6.117
	PTP5					PTP6				
B3LYP	6.402	9.335	16.817	26.152	-4.836	5.042	6.941	13.807	20.748	-4.602
CAM-B3LYP	3.568	3.772	11.562	15.335	-6.021	2.828	2.669	9.755	12.423	-5.762
B3PW91	6.716	9.875	17.542	27.417	-4.930	5.310	7.388	14.438	21.825	-4.695
PBEPBE	10.974	18.464	25.734	44.199	-4.237	8.514	13.839	20.549	34.388	-4.016
WB97XD	2.859	2.476	10.296	12.772	-6.584	2.279	1.698	8.8	10.498	-6.318

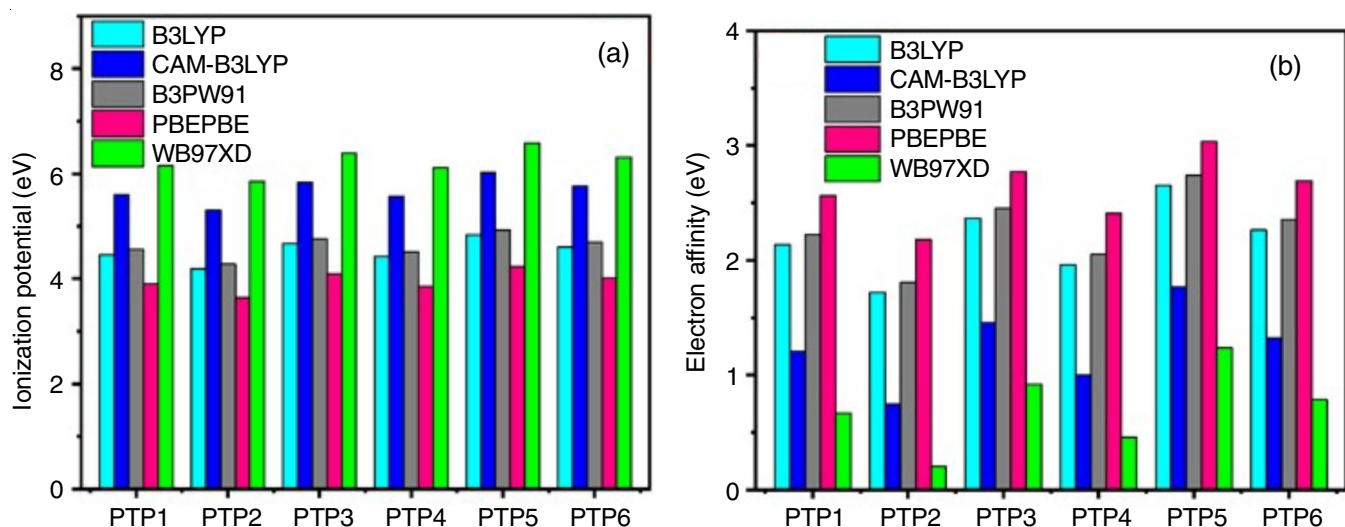


Fig. 6. Ionization potential and electron affinity of PTP molecules at several functionals B3LYP, CAM-B3LYP, B3PW91, PBEPBE and WB97XD using TD-DFT/6-311(d,p) level

and electron affinity increase if the core benzene ring of pentacene in PTP1 and PTP2 is replaced by nitrogen containing cyclic rings *i.e.* pyridine and pyrazine (PTP3, PTP4, PTP5 and PTP6). The outcomes demonstrate that the PTP5 and PTP2 molecules are good donor and acceptor because they exhibit a small ionization potential and high electron affinity among all the PTP derivatives (Table-3).

Electronegativity and chemical potential: The electronegativity determines a molecule's tendency to attract electrons, whereas chemical potential represents an electron's desire to escape and is related to molecular electronegativity. The higher the electronegativity, the greater the tendency to attract an electron, but the lower the chemical potential, the more difficult it is to lose an electron but easier to gain one. The electronegativity and chemical potential of PTP derivatives in the B3LYP func-

tional are as follows: $PTP2 < PTP4 < PTP1 < PTP6 < PTP3 < PTP5$ and $PTP2 > PTP4 > PTP1 > PTP6 > PTP3 > PTP5$. In CAM-B3LYP, B3PW91, PBEPBE and WB97XD functionals, the electronegativity and chemical potential are ordered in the same pattern as in the B3LYP functional. The $-NH$ group is switched from inward (PTP1, PTP3 and PTP5) to outward (PTP2, PTP4 and PTP6), which decreases the electronegativity and increase the chemical potential (Fig. 7). It suggests that more difficult to attract and gain an electron an electron if the position of the $-NH$ group is altered at the periphery of pentacene. Increased values of electronegativity and decrease the values of chemical potential if the core benzene ring of pentacene in PTP1 and PTP2 is replaced by nitrogen containing cyclic rings *i.e.* pyridine and pyrazine (PTP3, PTP4, PTP5 and PTP6) (Table-3). The outcomes demonstrate that PTP5 molecule has

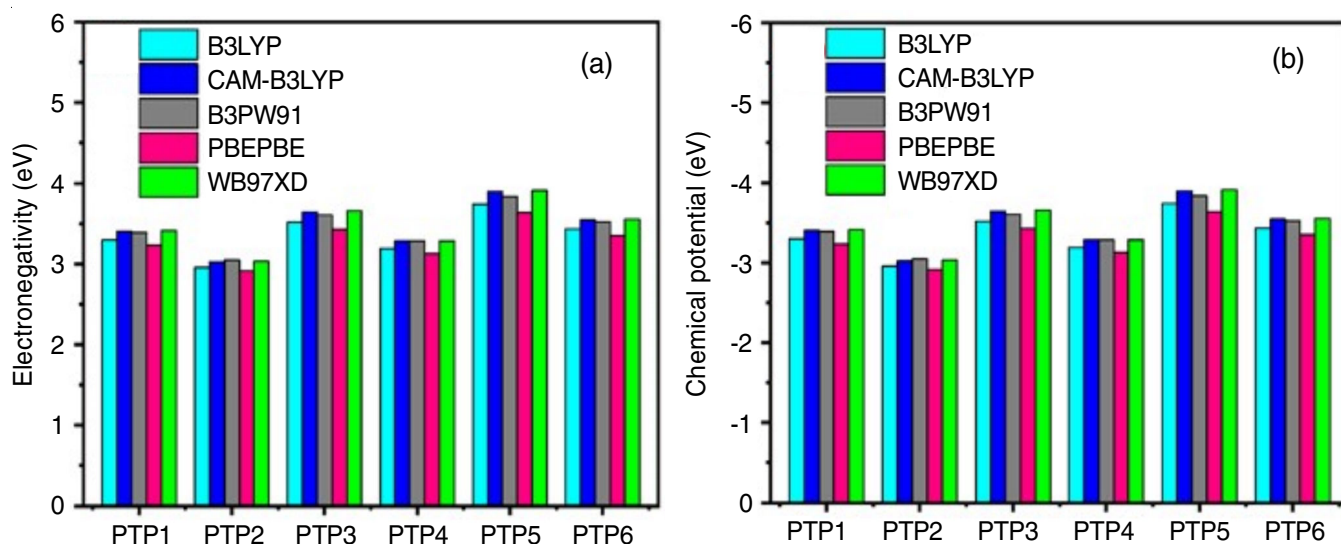


Fig. 7. Electronegativity and chemical potential of PTP molecules at several functionals B3LYP, CAM-B3LYP, B3PW91, PBEPBE and WB97XD using TD-DFT/6-311(d,p) level

greater tendency to attract and gain an electron easily because it exhibits low chemical potential and high electronegativity values among all the PTP molecules.

Hardness and softness: The HOMO-LUMO energy gap is directly related to the chemical hardness. A harder molecule is less reactive and more stable, which reduces the ability of charge transfer. Chemical softness, on the other hand, has an inverse relationship with hardness. A molecule becomes less stable and more reactive as its softness increases, which enhances charge transfer tendency. The hardness and softness at B3LYP, CAM-B3LYP, B3PW91, PBEPBE and WB97XD functionals in the gaseous phase. The hardness and softness of PTP molecules in the B3LYP functional are as follows: $PTP2 > PTP4 > PTP6 > PTP1 > PTP3 > PTP5$ and $PTP2 < PTP4 < PTP6 < PTP1 < PTP3 < PTP5$. In CAM-B3LYP, B3PW91, PBEPBE and WB97XD functionals, the hardness and softness are ordered in the same pattern as in the B3LYP functional. The -NH group switches from inward (PTP1, PTP3 and PTP5) to outward (PTP2, PTP4 and PTP6), decreasing softness while increasing hardness. It suggests that changing the position of the -NH group at the periphery of pentacene reduces charge transfer tendency and reactivity. The results show that among all the molecules based on PTP molecules, PTP2 molecule is less reactive and more stable, which reduces the charge transfer ability due to its hard character (Table-3). Among all the designed molecules, PTP5 molecule is the softest, least stable and most reactive, which increases the charge transfer ability.

Electrophilic character, electrodonating power, electro-accepting power and nucleophilic character: Electrophilicity index, electrodonating power, electroaccepting power, nucleophilicity index and electrophilicity at B3LYP, CAM-B3LYP, B3PW91, PBEPBE and WB97XD functionals in the gaseous phase. A molecule with a high electrophilicity index and net electrophilicity values has a good electrophilic character, whereas a high nucleophilicity index value indicates a superior nucleophilic character (Table-4). In the B3LYP functional, the order of electrophilicity index, electrodonating power, electro-

accepting power and net electrophilicity of PTP molecules are as follows: $PTP2 < PTP4 < PTP1 < PTP6 < PTP3 < PTP5$ while the order of nucleophilicity index is as occur: $PTP5 < PTP3 < PTP6 < PTP1 < PTP4 < PTP2$. In CAM-B3LYP, B3PW91, PBEPBE and WB97XD functionals, the electrophilicity index, electrodonating power, electroaccepting power, net electrophilicity and nucleophilicity index are ordered in the same pattern as in the B3LYP functional. The -NH group is switched from inward (PTP1, PTP3 and PTP5) to outward (PTP2, PTP4 and PTP6), which decreases the electrophilicity index, electrodonating power, electroaccepting power and net electrophilicity while increases the nucleophilicity index. It implies that altering the location of NH group on the perimeter of pentacene will increase the nucleophilic and decrease the electrophilic character. Increased the values of electrophilicity index, electrodonating power, electroaccepting power and net electrophilicity while decreasing the values of nucleophilicity index if the core benzene ring of pentacene in PTP1 and PTP2 is replaced by nitrogen containing cyclic rings *i.e.* pyridine and pyrazine (PTP3, PTP4, PTP5 and PTP6). Among all the designed molecules based on PTP, PTP5 molecule shows the highest electrophilicity index, electrodonating power, electroaccepting power and net electrophilicity values, indicating that it has a better ability to attract and gain an electron with ease. However, out of all the designed molecules, PTP2 molecule has a good nucleophilic character due to its large nucleophilicity index values.

Molecular electrostatic potentials mapping: The molecular electrostatic potential mapping is an important aspect of understanding the reactivity sites for electrophilic and nucleophilic attack [44-47]. By utilizing the DFT technique at 6-311 (d,p) basis set and the B3LYP functional, the mapping of the molecular electrostatic potential of PTP molecules was determined. The electrostatic potential mapping is visible on the surface of PTP based on red and blue hues (Fig. 8). The colour blue represents the positive electrostatic potential or electron-poor site, whereas red represents the negative electrostatic potential or electron-rich site. As a result, blue (positive electro-

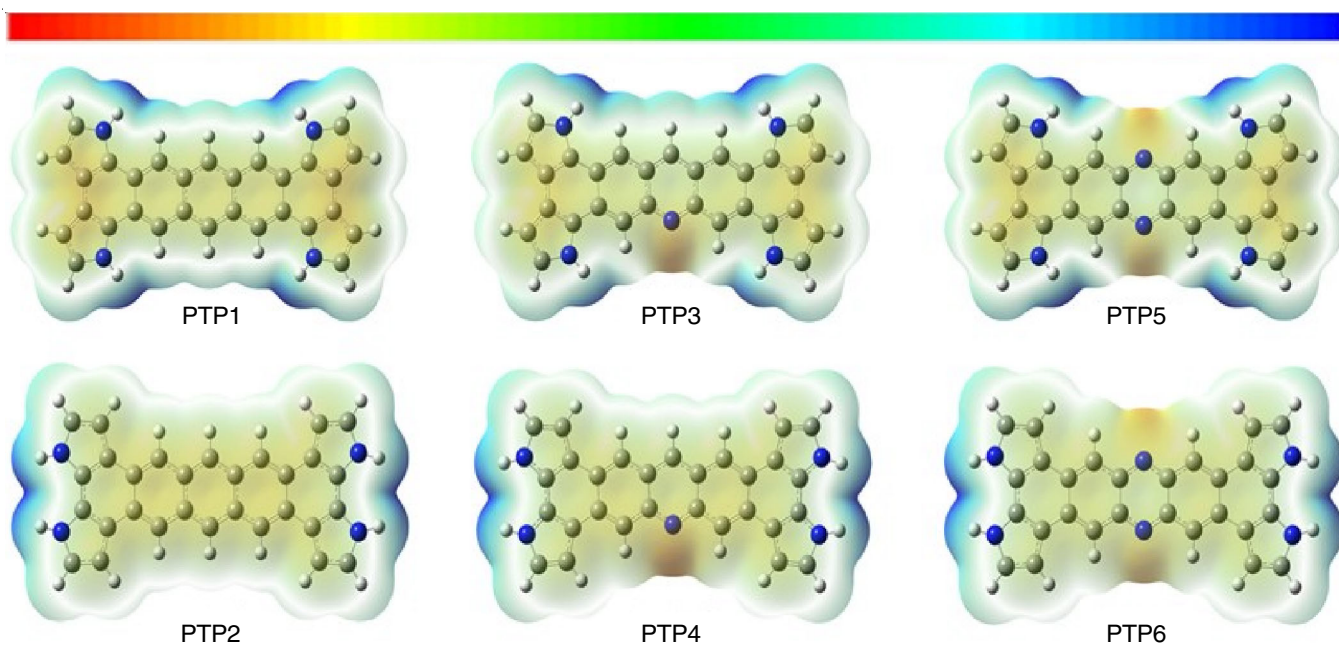


Fig. 8. Molecular electrostatic potential mapping of PTP molecules using DFT/B3LYP/6-311(d,p) level

static potential) site prefers a nucleophilic attack, whereas red (negative electrostatic potential) site prefers an electrophilic attack.

The range of colour coding in the mapping for PTP molecules is listed below:

PTP1 = $-5.710e^{-2}$ (deep red) to $+5.710e^{-2}$ (deep blue)

PTP2 = $-7.767e^{-2}$ (deep red) to $+7.767e^{-2}$ (deep blue)

PTP3 = $-5.951e^{-2}$ (deep red) to $+5.951e^{-2}$ (deep blue)

PTP4 = $-7.894e^{-2}$ (deep red) to $+7.894e^{-2}$ (deep blue)

PTP5 = $-5.533e^{-2}$ (deep red) to $+5.533e^{-2}$ (deep blue)

PTP6 = $-8.100e^{-2}$ (deep red) to $+8.100e^{-2}$ (deep blue)

The analysis of molecular electrostatic potential mapping for PTP molecules (Fig. 8) illustrates that red colour (negative electrostatic potential site) is located on the nitrogen atom present in pyridine (PTP3 and PTP4) and pyrazine rings (PTP5 and PTP6), indicating that this site is preferred for an electrophilic attack. On the other hand, the blue colour (positive electrostatic potential site) is concentrated on the hydrogen atom attached to the nitrogen *i.e.*, the $-NH$ group of the pyrrole rings at the peripheral region of pentacene, implying that this site is more appropriate for a nucleophilic attack in PTP molecules.

Optical properties: To understand the optical properties of PTP molecules, the absorption wavelength, oscillation strength, electronic transition energy and main transition with their percentage contribution were estimated using TD-DFT/6-311(d,p). To further investigate the effect of various functionals on optical properties, TD-DFT calculations were done by various B3LYP, CAM-B3LYP, B3PW91, PBEPBE and WB97XD functionals utilizing DFT-optimized structures PTP molecules which are shown in Table-5. The trend of absorption maximum wavelength in B3LYP and WB97XD is PTP6 > PTP5 > PTP3 > PTP1 > PTP4 > PTP2 and PTP6 > PTP2 > PTP5 > PTP3 > PTP1 > PTP4 whereas order of the HOMO-LUMO energy gap in PBEPBE is: PTP2 > PTP4 > PTP1 > PTP6 > PTP3 > PTP5. The order of the absorption maximum wavelength in CAM-

B3LYP, B3PW91 and PBEPBE functionals is the same as in the B3LYP functional (Fig. 9). From the TD-DFT calculation results, the absorption wavelength for the PTP1 compound is at 752 nm with 0.004 oscillating strength and 1.649 eV electronic transition energy due to HOMO to LUMO (98%) transition. A second excitation was at 538 nm with 0.239 oscillating strength and 2.306 eV electronic transition energy due to HOMO-1 to LUMO (82%) transition. For PTP2 compound, the calculated absorption wavelength is observed at 687 nm with 0.021 oscillating strength and 1.805 eV electronic transition energy due to HOMO to LUMO (96%) transition while second excitation was at 448 nm with 0.098 oscillating strength and 2.765 eV electronic transition energy due to HOMO-3 to LUMO (69%) and HOMO to LUMO+2 (30%) transitions (Fig. 9). In PTP1 and PTP2 (position of $-NH$ group replacing inward to outward) compounds, the absorption maximum was observed at 538 nm and 448 nm *i.e.*, towards the shorter wavelength. The position of the $-NH$ group is switched from inward (PTP1, PTP3 and PTP5) to outward (PTP2, PTP4 and PTP6), which shifts absorption maximum towards the shorter wavelength for PTP1 and PTP3 while observed towards the longer absorption maximum wavelength in case of PTP5. Further, if the core benzene ring of pentacene in PTP1/PTP2 is replaced by nitrogen containing cyclic rings *i.e.* pyridine and pyrazine *i.e.* PTP3/PTP4, PTP5/PTP6, then absorption maximum was observed at 558 nm/458 nm and 590 nm/794 nm. The absorption maximum wavelength range lies in visible from 447-794 nm in PBEPBE functional. Among all the PTP molecules, the PTP6 molecule shows the largest absorption maximum wavelength (lower excitation energy) among all the investigated compounds.

Thermodynamic properties: The DFT/B3LYP/6-311(d,p) methodology was used to determine the thermodynamic properties at 1 atm pressure and 298.15 K temperature of PTP molecules. These properties included zero-point vibrational energies

TABLE-5
OPTICAL PROPERTIES OF DESIGNED PTP MOLECULES AT SEVERAL FUNCTIONALS B3LYP, CAM-B3LYP, B3PW91, PBEPBE AND WB97XD USING TD-DFT/6-311(d,p) LEVEL

Functional	λ_{abs}	f	E_{ex}	MT (%C _i)	λ_{abs}	f	E_{ex}	MT (%C _i)	
PTP1					PTP2				
B3LYP	630	0.009	1.968	H→L (100%)	583	0.036	2.128	H→L (99%)	
	457	0.261	2.712	H-2→L (80%)	399	0.096	3.109	H-2→L (67%), H→L+2 (32%)	
CAM-B3LYP	514	0.022	2.411	H L (98%)	485	0.068	2.557	H→L (97%)	
	392	0.218	3.165	H-1→L (69%), H→L+1 (23%)	362	0.078	3.422	H-2→L (60%), H→L+2 (33%)	
B3PW91	628	0.009	1.974	H→L (100%)	581	0.037	2.135	H→L (100%)	
	456	0.261	2.719	H-2→L (80%)	397	0.092	3.120	H-2 L (67%), H L+2 (32%)	
PBEPBE	752	0.004	1.649	H→L (98%)	687	0.021	1.805	H→L (96%)	
	538	0.239	2.306	H-1→L (82%)	448	0.098	2.765	H-3→L (69%), H→L+2 (30%)	
WB97XD	497	0.026	2.496	H→L (96%)	471	0.075	2.633	H→L (96%)	
	383	0.203	3.233	H-1→L (65%), H→L+1 (23%)	358	0.074	3.464	H-2→L (58%), H→L+2 (32%)	
PTP3					PTP4				
B3LYP	648	0.006	1.913	H→L (100%)	596	0.031	2.081	H→L (99%)	
	514	0.002	2.413	H-1→L (97%)	485	0.002	2.556	H-1→L (99%)	
	473	0.47	2.621	H-2→L (86%)	405	0.313	3.061	H-2→L (79%)	
CAM-B3LYP	520	0.016	2.385	H→L (97%)	485	0.061	2.555	H→L (97%)	
	408	0.025	3.038	H-2→L (62%), H-1→L (30%)	380	0.005	3.264	H-1→L (90%)	
	402	0.518	3.084	H-2→L (28%), H-1→L (53%)	366	0.338	3.386	H-2→L (74%)	
B3PW91	647	0.006	1.918	H→L (100%)	594	0.031	2.087	H→L (99%)	
	513	0.002	2.418	H-1→L (97%)	484	0.002	2.56	H-1→L (99%)	
	472	0.472	2.627	H-2→L (86%)	404	0.311	3.072	H-2→L (79%)	
PBEPBE	782	0.003	1.586	H→L (98%)	717	0.017	1.729	H→L (96%)	
	631	0.001	1.966	H-1→L (97%)	606	0.001	2.047	H-1→L (98%)	
	558	0.371	2.223	H-2→L (87%)	458	0.262	2.708	H-2→L (79%)	
WB97XD	501	0.019	2.477	H→L (96%)	470	0.068	2.639	H→L (95%)	
	394	0.309	3.149	H-2→L (27%)	366	0.007	3.385	H-1→L+2 (84%)	
	392	0.231	3.159	H-1→L (56%), H-2→L (60%)	362	0.335	3.429	H-2→L (73%)	
PTP5					PTP6				
B3LYP	703	0.004	1.764	H→L (100%)	646	0.023	1.919	H→L (100%)	
	500	0.636	2.478	H-2→L (92%)	434	0.001	2.856	H-4→L (99%)	
CAM-B3LYP	553	0.011	2.241	H→L (97%)	513	0.048	2.417	H→L (96%)	
	423	0.801	2.929	H-1→L (87%)	381	0.001	3.25	H-6→L (94%)	
B3PW91	702	0.004	1.766	H→L (100%)	645	0.023	1.922	H→L (100%)	
	500	0.641	2.482	H-2→L (92%)	442	0.001	2.807	H-4→L (99%)	
PBEPBE	858	0.001	1.445	H→L (98%)	794	0.012	1.563	H→L (97%)	
	590	0.48	2.102	H-2→L (90%)	550	0.001	2.256	H-2→L (100%)	
WB97XD	531	0.013	2.337	H→L (96%)	495	0.054	2.506	H→L (94%)	
	414	0.812	2.998	H-1→L (84%)	389	0.001	3.184	H-4→L (94%)	

(ZPVE in kcal mol⁻¹), thermal energies (E_T in kcal mol⁻¹), heat capacity at constant volume (C_v in cal mol⁻¹ K⁻¹), entropy (S in cal mol⁻¹ K⁻¹), enthalpies (H in kcal mol⁻¹) and Gibbs free energies (G in kcal mol⁻¹). The results of thermodynamic properties are presented in Table-6. The order of zero-point vibrational energies, thermal energies and entropy are: PTP6 < PTP5 < PTP4 < PTP3 < PTP2 < PTP1 and PTP5 < PTP3 < PTP6 < PTP1 <

PTP4 < PTP2 while trend of heat capacity at constant volume, enthalpies and Gibbs free energies are as follows: PTP5 < PTP6 < PTP3 < PTP4 < PTP1 < PTP2. The -NH group is switched from inward (PTP1, PTP3 and PTP5) to outward (PTP2, PTP4 and PTP6), which decreases the zero-point vibrational energies and thermal energies while increasing the heat capacity at constant volume, entropy, enthalpies and Gibbs free energies. If

TABLE-6
THERMODYNAMIC PROPERTIES OF DESIGNED PTP MOLECULES COMPUTED USING DFT/B3LYP/6-311(d,p) LEVEL

Compounds	ZPVE	E_T	C_v	S	H	G
PTP1	251.978	266.982	102.013	162.882	-861558	-861607
PTP2	251.677	266.866	102.63	164.088	-861553	-861602
PTP3	244.788	259.636	100.77	161.993	-871635	-871683
PTP4	244.441	259.487	101.459	163.259	-871629	-871678
PTP5	237.398	252.107	99.715	161.069	-881709	-881757
PTP6	236.985	251.912	100.512	162.546	-881703	-881751

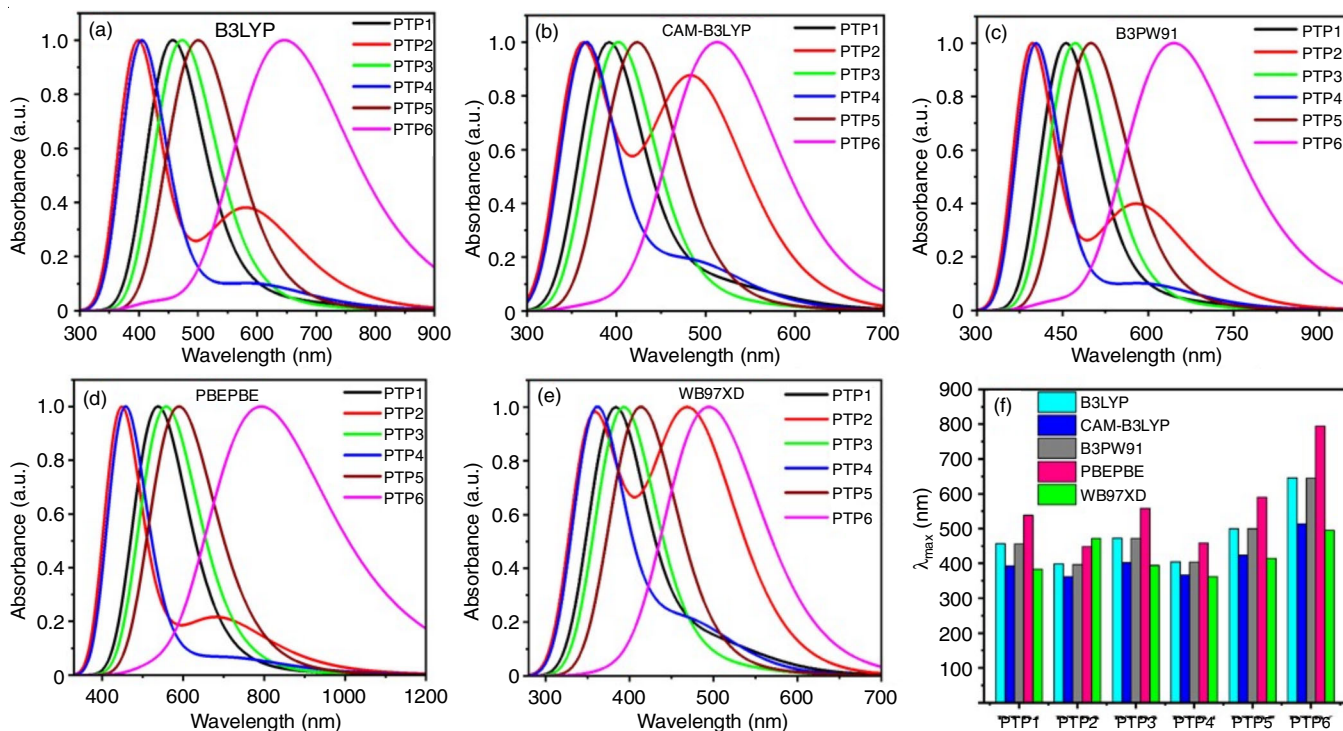


Fig. 9. Absorption spectra (a, b, c, d, e) and absorption maxima wavelength (f) of PTP molecules at several functionals B3LYP, CAM-B3LYP, B3PW91, PBEPBE and WB97XD using DFT/6-311(d,p) level

the core benzene ring of pentacene in PTP1 and PTP2 is replaced by nitrogen containing cyclic rings *i.e.* pyridine and pyrazine (PTP3, PTP4, PTP5 and PTP6) then thermodynamic properties decrease.

Conclusion

In this work, DFT and TD-DFT methodology at 6-311 (d,p) basis set have been used to perform all the calculations for the theoretical study of the electronic properties, reactivity indices, optical and thermodynamic properties of pentacene-tetrapyrrole (PTP) molecules at several functionals B3LYP, CAM-B3LYP, B3PW91, PBEPBE and WB97XD. Because of the smallest HOMO-LUMO energy gap, the PTP5 molecule possesses the strongest charge transfer ability among all the designed PTP molecules. The PTP5 and PTP2 molecules are effective donors and acceptors due to their low ionization potential as well as high electron affinity. The PTP5 molecule has a higher tendency to attract and gain electrons than any other pentacene-tetrapyrrole derivatives due to its low chemical potential and high electronegativity values. The PTP5 molecule is also the softest, least stable and most reactive, which increases its charge transfer capabilities. The PTP5 molecule has the highest electrophilicity index, electrodonating power, electro-accepting power and net electrophilicity values, indicating that it can attract and acquire electrons more easily. However, out of all the molecules based on pentacene-tetrapyrrole, PTP2 molecule has a good nucleophilic character due to its nucleophilicity index values. The absorption maximum wavelength range lies in visible from 447-794 nm (in PBEPBE functional). The PTP6 molecule shows the largest absorption maximum wavelength (lower excitation energy) among all the investigated

compounds. The results, in addition to this theoretical investigation, contribute to the development of new organic materials that contribute to the improvement of optoelectronic devices.

CONFLICT OF INTEREST

The authors declare that there is no conflict of interests regarding the publication of this article.

REFERENCES

- C. Sutton, J.S. Sears, V. Coropceanu and J.-L. Brédas, *J. Phys. Chem. Lett.*, **4**, 1919 (2013); <https://doi.org/10.1021/jz3021292>
- K. Bouchouit, Z. Sofiani, B. Derkowska, S. Abed, N. Benali-Cherif, M. Bakasse and B. Sahraoui, *Opt. Commun.*, **278**, 180 (2007); <https://doi.org/10.1016/j.optcom.2007.05.068>
- K. Bouchouit, Z. Essaidi, S. Abed, A. Migalska-Zalas, B. Derkowska, N. Benali-cherif, M. Mihaly, A. Meghea and B. Sahraoui, *Chem. Phys. Lett.*, **455**, 270 (2008); <https://doi.org/10.1016/j.cplett.2008.02.101>
- K. Bouchouit, H. Bougharraf, B. Derkowska-Zielinska, N. Benali-cherif and B. Sahraoui, *Opt. Mater.*, **48**, 215 (2015); <https://doi.org/10.1016/j.optmat.2015.07.035>
- F. Aziz, M. Hassan Sayyad, K. Sulaiman, B.H. Majlis, K.S. Karimov, Z. Ahmad and G. Sugandi, *Meas. Sci. Technol.*, **23**, 014001 (2012); <https://doi.org/10.1088/0957-0233/23/1/014001>
- M. Murugavelu, P.K.M. Imran, K.R. Sankaran and S. Nagarajan, *Mater. Sci. Semicond. Process.*, **16**, 461 (2013); <https://doi.org/10.1016/j.mssp.2012.08.001>
- Y. Che, X. Yang, G. Liu, C. Yu, H. Ji, J. Zuo, J. Zhao and L. Zang, *J. Am. Chem. Soc.*, **132**, 5743 (2010); <https://doi.org/10.1021/ja909797q>
- M. Guan, L. Li, G. Cao, Y. Zhang, B. Wang, X. Chu, Z. Zhu and Y. Zeng, *Org. Electron.*, **12**, 2090 (2011); <https://doi.org/10.1016/j.orgel.2011.09.003>

9. H.-R. Tseng, H. Phan, C. Luo, M. Wang, L.A. Perez, S.N. Patel, L. Ying, E.J. Kramer, T.-Q. Nguyen, G.C. Bazan and A.J. Heeger, *Adv. Mater.*, **26**, 2993 (2014); <https://doi.org/10.1002/adma.201305084>
10. L. Xiao-Hong, C. Hong-Ling, Z. Rui-Zhou and Z. Xian-Zhou, *Spectrochim. Acta A Mol. Biomol. Spectrosc.*, **137**, 321 (2015); <https://doi.org/10.1016/j.saa.2014.08.036>
11. M. Yoosuf Ameen, T. Abhijith, S. De, S.K. Ray and V.S. Reddy, *Org. Electron.*, **14**, 554 (2013); <https://doi.org/10.1016/j.orgel.2012.12.012>
12. Z. Liu, M. Kobayashi, B.C. Paul, Z. Bao and Y. Nishi, *Phys. Rev. B Condens. Matter Mater. Phys.*, **82**, 035311 (2010); <https://doi.org/10.1103/PhysRevB.82.035311>
13. M. Ball, Y. Zhong, Y. Wu, C. Schenck, F. Ng, M. Steigerwald, S. Xiao and C. Nuckolls, *Acc. Chem. Res.*, **48**, 267 (2015); <https://doi.org/10.1021/ar500355d>
14. W. Pisula, X. Feng and K. Müllen, *Chem. Mater.*, **23**, 554 (2011); <https://doi.org/10.1021/cm102252w>
15. Z. Sun, Q. Ye, C. Chi and J. Wu, *Chem. Soc. Rev.*, **41**, 7857 (2012); <https://doi.org/10.1039/c2cs35211g>
16. W. Chen, X. Li, G. Long, Y. Li, R. Ganguly, M. Zhang, N. Aratani, H. Yamada, M. Liu and Q. Zhang, *Angew. Chem.*, **130**, 13743 (2018); <https://doi.org/10.1002/ange.201808779>
17. J. Li, S. Chen, Z. Wang and Q. Zhang, *Chem. Rec.*, **16**, 1518 (2016); <https://doi.org/10.1002/tcr.201600015>
18. R. Rieger and K. Müllen, *J. Phys. Org. Chem.*, **23**, 315 (2010); <https://doi.org/10.1002/poc.1644>
19. A. Narita, X.-Y. Wang, X. Feng and K. Müllen, *Chem. Soc. Rev.*, **44**, 6616 (2015); <https://doi.org/10.1039/C5CS00183H>
20. Z. Sun and J. Wu, *J. Mater. Chem.*, **22**, 4151 (2012); <https://doi.org/10.1039/C1JM14786B>
21. P.-Y. Gu, Y. Zhao, J.-H. He, J. Zhang, C. Wang, Q.-F. Xu, J.-M. Lu, X.W. Sun and Q. Zhang, *J. Org. Chem.*, **80**, 3030 (2015); <https://doi.org/10.1021/jo5027707>
22. P.Y. Gu, Z. Wang, G. Liu, H. Yao, Z. Wang, Y. Li, J. Zhu, S. Li and Q. Zhang, *Chem. Mater.*, **29**, 4172 (2017); <https://doi.org/10.1021/acs.chemmater.7b01318>
23. L. Ji, A. Friedrich, I. Krummenacher, A. Eichhorn, H. Braunschweig, M. Moos, S. Hahn, F.L. Geyer, O. Tverskoy, J. Han, C. Lambert, A. Dreuw, T.B. Marder and U.H.F. Bunz, *J. Am. Chem. Soc.*, **139**, 15968 (2017); <https://doi.org/10.1021/jacs.7b09460>
24. M. Richter, K.S. Schellhammer, P. Machata, G. Cuniberti, A. Popov, F. Ortman, R. Berger, K. Müllen and X. Feng, *Org. Chem. Front.*, **4**, 847 (2017); <https://doi.org/10.1039/C7QO00180K>
25. Z. Wang, P. Gu, G. Liu, H. Yao, Y. Wu, Y. Li, G. Rakesh, J. Zhu, H. Fu and Q. Zhang, *Chem. Commun.*, **53**, 7772 (2017); <https://doi.org/10.1039/C7CC03898D>
26. A. Mateo-Alonso, *Chem. Soc. Rev.*, **43**, 6311 (2014); <https://doi.org/10.1039/C4CS00119B>
27. U.H.F. Bunz, *Acc. Chem. Res.*, **48**, 1676 (2015); <https://doi.org/10.1021/acs.accounts.5b00118>
28. A. Irfan, A.R. Chaudhary, S. Muhammad, A.G. Al-Sehemi, H. Bo, M.W. Mumtaz and M.A. Qayyum, *Results Phys.*, **11**, 599 (2018); <https://doi.org/10.1016/j.rinp.2018.09.052>
29. V.M. Vidya and P. Chetti, *J. Phys. Org. Chem.*, **34**, e4128 (2021); <https://doi.org/10.1002/poc.4128>
30. N.N. Tri, L.V. Duong and M.T. Nguyen, *Mater. Today Commun.*, **24**, 101054 (2020); <https://doi.org/10.1016/j.mtcomm.2020.101054>
31. M.J. Frisch, G.W. Trucks, H.B. Schlegel, G.E. Scuseria, M.A. Robb, J.R. Cheeseman, G. Scalmani, V. Barone, B. Mennucci, G.A. Petersson, H. Nakatsuji, M. Caricato, X. Li, H.P. Hratchian, A.F. Izmaylov, J. Bloino, G. Zheng, J.L. Sonnenberg, M. Hada, M. Ehara, K. Toyota, R. Fukuda, J. Hasegawa, M. Ishida, T. Nakajima, Y. Honda, O. Kitao, H. Nakai, T. Vreven, J.A. Montgomery Jr., J.E. Peralta, F. Ogliaro, M. Bearpark, J.J. Heyd, E. Brothers, K.N. Kudin, V.N. Staroverov, R. Kobayashi, J. Normand, K. Raghavachari, A. Rendell, J.C. Burant, S.S. Iyengar, J. Tomasi, M. Cossi, N. Rega, N.J. Millam, M. Klene, J.E. Knox, J.B. Cross, V. Bakken, C. Adamo, J. Jaramillo, R. Gomperts, R.E. Stratmann, O. Yazyev, A.J. Austin, R. Cammi, C. Pomelli, J.W. Ochterski, R.L. Martin, K. Morokuma, V.G. Zakrzewski, G.A. Voth, P. Salvador, J.J. Dannenberg, S. Dapprich, A.D. Daniels, Ö. Farkas, J. B. Foresman, J.V. Ortiz, J. Cioslowski and D.J. Fox, Gaussian 09, Gaussian, Inc., Wallingford CT (2009).
32. N.M. O'boyle, A.L. Tenderholt and K.M. Langner, *J. Comput. Chem.*, **29**, 839 (2008); <https://doi.org/10.1002/jcc.20823>
33. O.E. Oyeneyin, *Phys. Sci. Int. J.*, **16**, 1 (2017); <https://doi.org/10.9734/PSIJ/2017/36555>
34. M.F. Khan, R.B. Rashid, M.A. Hossain and M.A. Rashid, *Dhaka Univ. J. Pharm. Sci.*, **16**, 1 (2017); <https://doi.org/10.3329/dujps.v16i1.33376>
35. K.K. Srivastava, S. Srivastava and T. Alam, *Pelagia Res. Libr.*, **5**, 288 (2014).
36. J.L. Gázquez, A. Cedillo and A. Vela, *J. Phys. Chem. A*, **111**, 1966 (2007); <https://doi.org/10.1021/jp065459f>
37. P.K. Chattaraj, A. Chakraborty and S. Giri, *J. Phys. Chem. A*, **113**, 10068 (2009); <https://doi.org/10.1021/jp904674x>
38. R. Contreras, J. Andres, V.S. Safont, P. Campodonico and J.G. Santos, *J. Phys. Chem. A*, **107**, 5588 (2003); <https://doi.org/10.1021/jp0302865>
39. A. Cedillo, R. Contreras, M. Galván, A. Aizman, J. Andrés and V.S. Safont, *J. Phys. Chem. A*, **111**, 2442 (2007); <https://doi.org/10.1021/jp068459o>
40. P. Jaramillo, P. Pérez, R. Contreras, W. Tiznado and P. Fuentealba, *J. Phys. Chem. A*, **110**, 8181 (2006); <https://doi.org/10.1021/jp057351q>
41. P. Campodonico, J.G. Santos, J. Andres and R. Contreras, *J. Phys. Org. Chem.*, **17**, 273 (2004); <https://doi.org/10.1002/poc.719>
42. T. Karakurt, M. Dinçer, A. Çetin and M. Sekerci, *Spectrochim. Acta A Mol. Biomol. Spectrosc.*, **77**, 189 (2010); <https://doi.org/10.1016/j.saa.2010.05.006>
43. J. Zhang, Y.-H. Kan, H.-B. Li, Y. Geng, Y. Wu and Z.-M. Su, *Dyes Pigments*, **95**, 313 (2012); <https://doi.org/10.1016/j.dyepig.2012.05.020>
44. R.G. Parr, R.A. Donnelly, M. Levy and W.E. Palke, *J. Chem. Phys.*, **68**, 3801 (1978); <https://doi.org/10.1063/1.436185>
45. R.G. Pearson, *J. Am. Chem. Soc.*, **85**, 3533 (1963); <https://doi.org/10.1021/ja00905a001>
46. R.G. Parr and R.G. Pearson, *J. Am. Chem. Soc.*, **105**, 7512 (1983); <https://doi.org/10.1021/ja00364a005>
47. R.G. Parr, L. Szentpály and S. Liu, *J. Am. Chem. Soc.*, **121**, 1922 (1999); <https://doi.org/10.1021/ja983494x>